ALKALI RESISTANCE TESTING METHODOLOGY AND DEVELOPMENT: FOCUS ON MULLITE BASED CASTABLES

K. Haines*, K. Byrd and D. Lankard

Allied Mineral Products, Inc, Columbus, OH 43221

ABSTRACT

Aluminosilicate refractories, which are widely used in alkali-rich environments, typically have a matrix that is close to mullite in composition. It is the matrix component that is most vulnerable to attack in service.

In this study, the "matrix" is identified as including the mix water and the solid constituents with a particle size less than 0.5 mm. The formulation of experimental compositions was done on a volume percent basis to account for differences in the specific gravity of the constituents. This approach fixes the volume percent of water and provides the means to replace any of the solid constituents with an equal volume of other refractory materials. Aided by the use of polished thin sections, characterization procedures provide for the generation of information on microstructural, chemical, and mineralogical changes of the matrix.

INTRODUCTION

Alkali attack of aluminosilicate castable refractories has been a long-term problem in the industry [1-3]. Alkali vapors can condense in available pore space and lead to either a corrosive melt or react to form solid phases that can lead to physical damage of the refractory due to volume expansion [4]. Overall, operation of aluminosilicate refractories in an alkali rich environment will negatively impact the service life of the refractory [3]. There are several approaches to reduce the detrimental effects of alkali attack. Compositionally, zircon can be added to the matrix to aid in resistance [5]. A physical properties-based approach could be to reduce the amount of available pore space in the refractory [6].

The crucible cup test is the common way to test refractory materials and their resistance to alkali rich conditions [4]. ASTM C987 replicates an aggressive glass melting furnace environment where the refractory is exposed to alkali vapors. This test is pass/fail based on visual observation of the refractory after exposure to vapors alone.

The primary focus of this paper is the procedure used for analyzing refractory crucibles after exposure to alkali slag and vapor for 24 hours. Instead of basing the failure of a refractory on a visual basis after exposure to alkali vapor alone, this procedure incorporates analytical methods to determine how aluminosilicate refractories behave in a corrosive environment.

Pre-test samples (before alkali exposure) and post-test crucibles (after alkali exposure) were subjected to both visual analysis and formal analytical testing in this study. The goal of the analytical testing was to determine the post-test corrosive phases formed, penetration depth of alkali phases into the refractory crucible, and how the use of specified raw materials affected the microstructure and its ability to withstand alkali attack.

EXPERIMENTAL METHODS

Mix Designs

All mix designs for the project were developed on a volume percent basis, including water. This approach takes the density of each mix component into

Submitted for peer review to *International Journal of Ceramic Engineering and Science*

consideration and controls the amount of water added. Two of the five mix designs were developed with the intent to produce pure mullite $3Al_2O_3 \cdot 2SiO_2$ while altering one raw material component (Table I). Mix 8M used calcined mullite (Kyanite Mining) while 8M60 used Mulcoa 60 (Imerys) in its place. The third mix design, 8MZr, contained 400 mesh zircon in place of the 325 mesh calcined mullite. The fourth mix design, 8MCM, was developed using 325 mesh aluminosilicate filler material as a cost-effective alternative. This filler includes ~5% zircon. The last mix design, 8MAl, is alumina rich relative to the other designs. This mix used tabular alumina as the 325 mesh component. The maximum grain size used for this study is 35 mesh.

Pre-fire procedure

Cast crucibles were cured at 55°C for 24 hours before demolding and drying at 100°C for an additional 24 hours. After drying, the crucibles were fired to 1620°C and held for 10 hours to ensure the formation of a mullite matrix.

Alkali testing

The pre-fired crucibles were filled with 20 grams of granular anhydrous sodium carbonate supplied by GFS. Lids of the same mix designs were adhered with a fused mullite based mortar. Crucibles were fired to 1370°C using a multi-step firing schedule. A dwell of 24-hours was prescribed to allow ample time for reaction of the alkali slag.

Analytical sample preparation

Both the pre-test and post-test samples were used for analytical testing and thin section creation. The post-test crucibles were then divided into quarters using a wet saw and allowed to dry at 100°C. These quartered crucibles were used to make representative samples for various tests.

Table I: Mullite based mix designs developed to be subjected to corrosion. These designs were created considering volume percent (Vol. %) and specific gravity (Sp. Gr.).

Mix Constituent	Sp Gr	8M	8M60	8MZr	8MAl	8MCM	Vol. %
Water	1.0	x	x	x	x	x	25.5
AB300	3.1	x	x	x	x	x	6.5
971U Fume	2.2	x	x	x	x	x	3.5
A3000 Al	3.8	x	x	x	x	x	18.4
35M Mullite	3.0	x		x	x	x	21.7
100M Mullite	3.0	x		x	x	x	9.4
325M Mullite	3.0	x					15.0
35M Mulcoa 60	2.8		x				21.7
100M Mulcoa 60	2.8		x				9.4
325M Mulcoa 60	2.8		x				15.0
400M Zircon	4.7			x			15.0
325M Tab. Al	3.5				x		15.0
325 CM	5.6					x	15.0

Thin Sections

Polished thin sections were made using the pre-test and post-test samples with a blue epoxy impregnate. The polished thin sections were requested without a cover slide so that energy dispersive spectroscopy (EDS) could be completed.

X-Ray Analysis

X-ray fluorescence (XRF) and x-ray diffraction (XRD) was completed for the pre-test and post-test specimens. A representative quarter from each post-test crucible was chosen for sample preparation. The reaction product from within the quartered sample's cavity was removed to be analyzed separate from the remainder of the crucible sample. Using the same quartered sample, the bottom was sectioned into layers approximately 0.6 cm thick for x-ray analysis.

EDS Analysis

Thin sections were evaluated using a Thermo Scientific Quattro ESEM equipped with an EDAX Octane Elect Energy Dispersive Spectroscopy (EDS) System. Electron Microscopy was performed at the Center for Electron Microscopy and Analysis (CEMAS) at The Ohio State University.

RESULTS

Pre-Test Results

8M, 8M60 and 8MZr shrank in volume after firing to 1620°C. Significant shrinkage (14%) was noted for 8M60. 8MCM and 8MAl both expanded by 4% relative to the other samples. The volume change was calculated by relating the fired density to the wet density measured during casting. 8MAl reports the highest porosity of 24%. 8M reports a porosity of 12%, 8MZr has 9% and 8MCM has 13%.

The pre-test chemical analysis for all samples indicated that 0.1-0.2% Na_2O

Table II: XRF analysis of the mix designs in wt. %. Pre-Test (PT), Layer 1 (L1), and Reaction Product (RP).

		Al_2O_3	Na_2O	SiO_2	ZrO_2	TiO_2	Fe_2O_3
8M	PT	72.9	0.1	25.8		0.7	0.4
	L1	71.7	1.9	25.4		0.7	0.4
	RP	51.7	31.7	15.6		0.5	0.4
8M60	PT	76.0	0.1	21.5		1.5	0.8
	L1	74.9	1.4	21.2	0.1	1.5	0.8
	RP	53.7	30.7	13.7		1.0	0.8
8MZr	PT	56.6	0.1	25.1	17.0	0.4	0.3
	L1	55.8	1.2	24.8	16.8	0.4	0.3
	RP	42.3	26.2	17.7	12.8	0.3	0.3
8MCM	PT	69.1	0.1	25.1	4.4	0.6	0.5
	L1	68.8	0.7	25.0	4.3	0.6	0.4
	RP	52.4	25.0	18.1	3.3	0.4	0.5
8MAl	PT	81.4	0.2	17.7		0.4	0.3
	L1	75.3	7.7	16.3		0.4	0.3
	RP	69.1	16.9	13.4		0.3	0.2

was present before the alkali run (Table II). Sample 8MAl has the lowest SiO_2 and highest Al_2O_3 percentage. Both 8MZr and 8MCM include the intentional addition of ZrO_2. XRD crystalline phase analysis is reported in Table III. All five samples were able to form mullite during firing. 8M, 8M60 and 8MAl contained mullite and corundum. In 8MZr, zircon is known to break down into silica and monoclinic ZrO_2[7] at the pre-test firing temperature, resulting in the identification of zirconia instead of zircon. Similarly, 8MCM identified the crystalline phases of mullite and zirconia.

In addition to XRF and XRD, the pre-test microstructure was observed using optical microscopy. Available pore space is easily identified due to the blue epoxy. The pre-test images served as a base comparison for the post-test thin sections.

Post-Test Results

Four of the five crucibles remained intact after firing with the sodium carbonate. These intact crucibles were cross sectioned for analysis (Fig. 1). 8MAl failed catastrophically (Fig. 2). The primary focus of post-test analytical testing is on the intact specimens.

Fig. 1. Post-test cross section of 8M.

Table III: XRD results of Pre-Test (PT), Layer 1 (L1), and Reaction Product (RP). *Gibbsite, ** Cristobalite, ***Natrolite, Mullite (M), Corundum (C), Zircon (ZA) and mono-ZrO_2 (m-Z).

		M	C	ZA	m-Z	β-Al	P05	P25	P35	P45	P55	Other
8M	PT	96.1	3.9									
	L1	93.8	2.4					3.8				
	RP						1.2	58.6	40.3			
8M60	PT	96.8	3.2									
	L1	92.4	4.8					2.8				
	RP	9.5	2.5				6.8	76.6				4.6*
8MZr	PT	82.9			17.1							
	L1	76.8		2.9	17					0.7		2.7**
	RP				9.4			31.3	35.6	23.7		
8MCM	PT	93.0			7							
	L1	92.7		0.8	5.4			1.0				
	RP		5.4		2.2	0.8		40.1	21.5			
8MAl	PT	73.2	26.8									
	L1	27.1	32.3			14.1			21.8		4.7	
	RP		2.8			25.3					12.7	5.7***

Fig. 2. Post-test 8MAl was unable to be cross sectioned.

Chemical Analysis

XRF was completed on the removed reaction product and the partitioned layers of all five samples. As expected, the majority of the sodium is found in the reaction product and in Layer 1 of the samples (Table II). The bottom layers of the samples do not show significant difference in chemistry and have been omitted from the results.

Phase Analysis

XRD analysis (Table III) of the crystalline phases was completed on Layer 1 (L1) and the reaction product (RP). Hydration occurred in 8M60 and 8MAl.

Aside from mullite, corundum and hydrated phases, the post-test samples included sodium aluminosilicate phases. They are primarily found in the reaction product but extend into Layer 1. These reaction phases can be described as $Al_{2-x}Na_{2-x}Si_xO_4$. The phase and crystal structure are directly related to the amount of SiO_2 present [8]. The phases found in this study will be described as Phase 05 (P05) ($Na_{1.95}Al_{1.95}Si_{0.05}O_4$), Phase 25 (P25) ($Na_{1.75}Al_{1.75}Si_{0.25}O_4$), Phase 35 (P35) ($Na_{1.65}Al_{1.65}Si_{0.35}O_4$), Phase 45 (P45) ($Na_{1.55}Al_{1.55}Si_{0.45}O_4$) and Phase 55 (P55) ($Na_{1.45}Al_{1.45}Si_{0.55}O_4$).

Zircon and cristobalite were identified in 8MZr. Relative to the pre-test, these phases were not previously present. The reaction product also contained the sodium aluminosilicate reaction phases described above.

8MCM also identified zircon relative to the pre-test analysis. The reaction product contained corundum (Al_2O_3) and diaoyudaoite ($Na_1Al_{11}O_{17}$). Diaoyudaoite has a β-alumina (β-Al) structure that is not found in the raw material used. β-alumina was also found in the 8MAl reaction product.

Optical Analysis

Transmitted light microscopy was used to observe the post-test thin sections. The crucibles have a distinct visual boundary (reaction interface) between the reaction product and the refractory (Fig. 3a).

Cross polarized microscopy was used to define the sodium aluminosilicate reaction phases found with the XRD. These crystals range from 10-70 μm in size and have low interference colors and exhibit twinning. 8M was found to have the largest crystals (70 μm) within the center of its reaction product. Additionally, monoclinic zirconia is identified in the reaction product of 8MZr and 8MCM.

Small needle shaped crystals, ~20-40 μm in length, can be found distributed through the 8MCM reaction product. These small needles also line the reaction interface of 8MCM.

8MCM has an irregular interface boundary with obvious destruction to the refractory. The thickness of this zone is up to 1 mm but varies throughout. The

boundary was disrupted by the elongate mineral formations. These elongated minerals are found in the other reaction interfaces of the other mix designs.

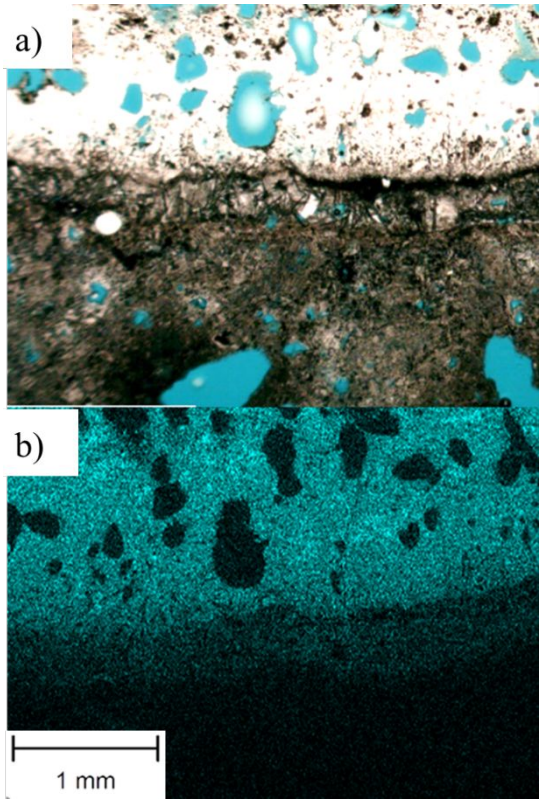

Fig. 3. a) Cross polarized microscopy at 25x magnification of 8M. b) Sodium map of the same area.

8M reaction interface has an average thickness 0.4 mm. The elongated phase dominates this zone in 8M (Fig.4) and run the thickness of this reaction layer. Separation and disruptions at the base of this zone is observed.

8M60 has a reaction interface that is 0.4-0.5 mm thick on average. This phase appears dark and glassy with evidence of the same elongated crystals observed in the other thin sections. While these crystals range in size, the elongated crystals are a max of 50 µm dispersed through the layer.

The reaction interface of 8MZr has a thickness of around 0.5 mm. The elongated mineral phase found in this interface ranged in size, the longest being 100 µm.

Scanning Electron Microscopy

Using EDS, elemental chemistries and element maps were obtained on the polished thin section samples (Fig. 3b). The area of interest analyzed included the reaction product, refractory, and the interface between. Five zones of approximately 1 mm by 0.3 mm, on each sample were selected for chemistry profiling to help visualize the sodium penetration through the sample.

DISCUSSION

Aluminosilicate raw material sources

8M and 8M60 were developed to be identical except for a single raw material. Pre-test microstructural analysis and XRD analysis shows that 8M and 8M60 had at least 96% mullite form after firing at 1620°C. Unfortunately, the amount of amorphous material could not be quantified by XRD. 8M60 used Mulcoa 60 as the base aggregate and had the lowest porosity with the highest shrinkage volumetrically. The lower porosity in the fired 8M60 sample may be attributed to the larger amount of amorphous material within the Mulcoa grains that lead to greater liquid phase sintering.

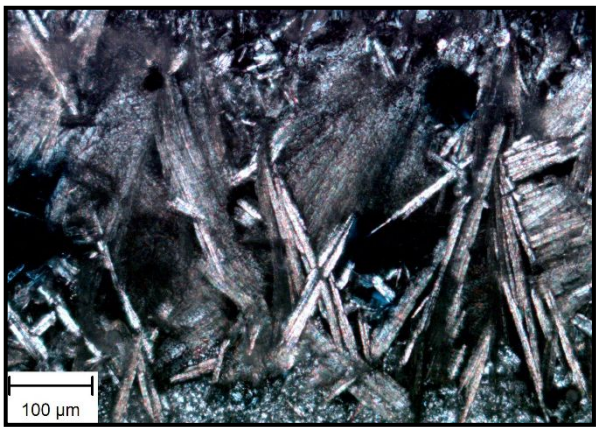

Fig. 4. Cross polarizing micrograph at 200x magnification of the elongate crystals found in 8M post-test.

The reaction zone

Every sample underwent some extent of corrosion after firing. Three distinct layers can be identified in the post-test thin sections: the reaction product, the reaction interface and unaltered refractory. XRD results revealed the presence of several Na-based phases as solid solutions

intermediate between sodium aluminate and nepheline. Five of these intermediate phases were found in the reaction products. Fig. 5 is the ternary phase diagram of the normalized pre-test chemistry of the five mixes and the normalized post-test reaction products of the mixes.

As the reaction progresses, the sodium aluminosilicate phases (dependent on silica content) change crystal shape [8]. The changes in crystal structure result in volume expansion within the reaction zone of the refractory. Because of the low porosity of the intact samples, most of the liquid sodium slag reaction occurred on the surface of t crucible minimizing the destructive effects of the volume expansion. However, some slag infiltrated into the available pore space where the sodium phases also begin to form.

The reaction interface of the analyzed samples can be defined optically. Separation of the reaction layer was observed as the refractory loses its structure due to the formation of the expansive

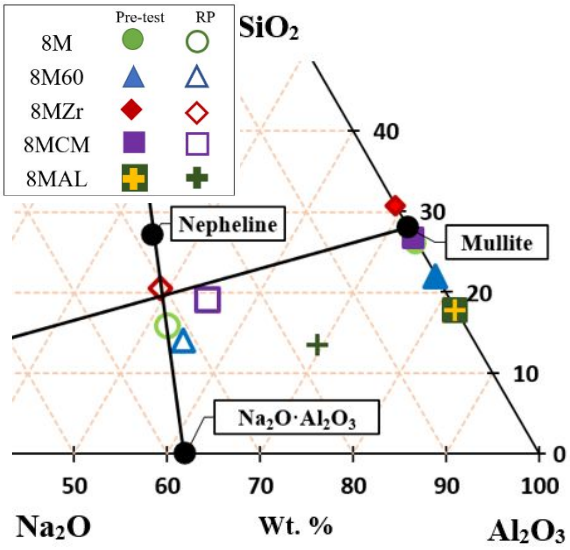

Fig. 5. Ternary diagram of the normalized pre-test chemistry and the post-test reaction products.

phases. In every sample, elongated crystals were observed in this interface layer that visually differ from the sodium

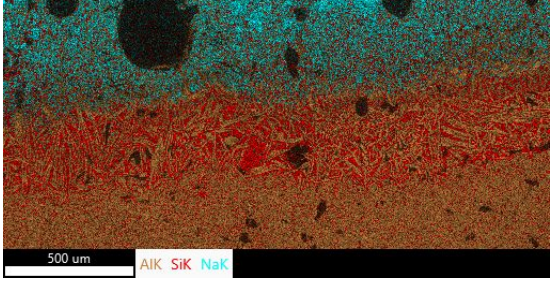

Fig. 6. Sodium map of 8M reaction zone. Al (orange), Si (red) and Na (blue).

aluminosilicate reaction phases found in the reaction product.

Further EDS analysis of these elongated crystals indicated that they are alumina rich with a low amount of sodium and are surrounded by sodium and silica (Fig. 6). These crystals have also been described in other published work [6]. It is suspected that these elongated crystals could be β-alumina. This is supported by the presence of β-alumina phases found via XRD in 8MCM and 8MAl.

Future studies will look further into the mechanisms at play within the reaction zone and will focus on these elongate phases that formed in addition to the sodium aluminosilicate reaction phases found in the reaction product.

The role of porosity

Accessible porosity provides conduits through which alkali vapors and liquid slags can move into the refractory. It is expected that reducing the pore space would in turn reduce the extent and severity of the distress caused by alkali interactions. The firing temperature of 1620°C was specifically selected to form mullite and liquid phases to help reduce porosity in the final product.

8MAl was the fifth mix designed for testing. This composition was designed to be alumina rich, limiting its ability to produce any liquid phases at the 1620°C firing temperature. It is suspected that this impacted the ability to sinter relative to the other samples. This is an example of a porous refractory (24%) that failed during alkali testing. In this case, the higher porosity has an obvious impact on the campaign life of the refractory.

CONCLUSIONS

This study used a new, defined procedure to aid in the research of reaction mechanisms involved with the corrosion of mullite-based castables. This procedure allowed for analytical analysis to define the reaction zones and the expansive phases present. The sodium aluminosilicate phases found were previously described [8]. These phases have now been related directly to the corrosion of aluminosilicate refractories that have been exposed to sodium carbonate. Additionally, understanding the mechanism of how these phases can form due to accessible porosity, or lack thereof, is crucial when considering the campaign life of refractory to be used in a corrosive environment.

ACKNOWLEDGMENTS

We would like to thank Concrete Research and Testing (CRT), the Center for Electron Microscopy and Analysis (CEMAS) and Wagner Petrographic in the aid of this research.

REFERENCES

1. Brachold N., Schaffoner S. and Aneziris C., "Investigation of alkali corrosion resistance of potassium aluminosilicates using statistical techniques," Ceram. Int., pp. 1447-1456, (2014).

2. Poirier J., "Reactions and Mechanisms of Corrosion," in Corrosion of Refractories-Testing and Characterization Methods, Göller-Verlag, pp. 229-336, (2017).

3. Zhao Y., Cheng G., Xiang Y., Long F. and Dong C., "Thermodynamic Study of the Corrosion of Refractories by Sodium Carbonate," Materials, (2018).

4. Poirier J., Quirmbach P. and Sax A., "Testing Methods for Corrosion," in Corrosion of Refractories: Testing and Characterization Methods, Baden-Baden, Goller Verlag GmbH, pp. 1-21, (2018).

5. Valenzuela-Gutierrez A., Lopez-Cuevas J., Gonzalez-Angeles A. and Pilalua-Diaz N., "Addition of ceramics materials to improve the corrosion resistance of alumina refractories," SN Appl. Sci., (2019).

6. Baspinar M. and Kara F., "Optimization of the corrosion behavior of mullite refractories against alkali vapor via ZrSiO4 addition to the binder phase," Ceramics-Silikaty, pp. 242-249, (2009).

7. Pavlik R., Holland H. and Payzant E., "Thermal Decomposition of Zircon Refractories," J. Am. Ceram. Soc., pp. 2930-2936, (2001).

8. Thompson J. G., Withers R. L., Melnitchenko A. and Palethorpe S. R., "Cristobolite-Related Phases in the NaAlO2-NaAlSiO4 System. I. Two Tetragonal and Two Orthorhombic Structures," Acta Crystallographica Section B, pp. 531-546, (1998).